Supplemental Materials for

"Defining the Internal Component of Atlantic Multidecadal Variability in a Changing Climate"

Clara Deser* and Adam S. Phillips

National Center for Atmospheric Research, Boulder, CO

Submitted to *Geophys. Res. Lett.* 17 April 2021

Revised 18 October 2021

* Corresponding author: Clara Deser (cdeser@ucar.edu)

Contents

This document contains four parts: 1) a note on the Trenberth and Shea (2006) method for estimating internal Atlantic Multidecadal Variability; 2) a list of references; 3) one Table (Table S1); and 4) 17 Figures (Figs. S1 – S17).

1. A note on the Trenberth and Shea (2006) method for estimating internal Atlantic Multidecadal Variability

Here, we clarify how Trenberth and Shea (2006; hereafter TS06) constructed their index of Atlantic Multidecadal Variability (AMV) and obtained the spatial pattern associated with this index. [This text should be read after the main paper, since it refers to results presented there.] TS06 defined their AMV Index as the timeseries of North Atlantic (NA) minus global (G; 60N-60S) SST based on annual mean data. Their aim in subtracting G from NA in their definition of AMV was to remove the externally-forced component from the Index. They also constructed a smoothed AMV Index by applying a weighted 13-point low-pass filter (half-power point at 16 years) to the raw AMV timeseries (see their Fig. 3 for both the raw and filtered AMV Index timeseries). Finally, they computed a global map of correlation coefficients between a gridded dataset of Surface Air Temperature (SAT) and the AMV Index. Although not explicitly stated in their paper, we have verified that their SAT correlation map (their Fig. 4) is based on *unfiltered* data for both the AMV Index timeseries and the gridded SAT field. The TS06 protocol for defining AMV has been widely adopted; however, unlike TS06, subsequent studies commonly apply a low-pass filter (typically a 10-year or 20-year running mean, or a Butterworth Filter or its equivalent with a half-power point between 10 and 20 years) to both the AMV Index timeseries and the gridded data field being correlated (or regressed) onto this timeseries.

Although the TS06 AMV Index is based on subtracting G from NA SST, we have verified that TS06 did not remove the global-mean from the gridded SAT dataset before computing the global correlation map of SAT with the AMV Index (their Fig. 4). In our application of the TS06 method

to future projections from initial-condition coupled climate model Large Ensembles, we find that inclusion of the global-mean in the gridded data (SST in our case) becomes problematic for the associated AMV spatial pattern estimated with their method.

Figures S15 and S16 show, for each model, the ensemble average of the AMV SST regression maps in each ensemble member, obtained by regressing the gridded SST data onto the NA-G SST Index. Figure S15 is based on the period 1950-2020 and Fig. S16 is based on the period 1950-2090; all data have been low-pass filtered with a 20-year Butterworth Filter. These regression maps may be compared with their counterparts shown in Figs. S1-9, which are based on subtracting the global-mean (60N-60S) SST from the gridded SST data prior to computing the regressions. In each model, the amplitudes of the regression coefficients based on the period 1950-2090 are clearly corrupted by inclusion of the global-mean in the gridded data, with values that are off-scale over much of the globe (Fig. S16). For example, CESM2 shows values < -3 over most of the globe outside of the subpolar NA (panel i in Fig. S16), compared to values between -1.6 and + 1.6 in the version based on removing the global-mean (panel b in Fig. S9) and between -0.8 and 0.8 based on the "Truth" (panel d in Fig. S9). Similar statements apply to all of the other model LEs examined in this study (Fig. S16). For the historical period 1950-2020 (Fig. S15), the regression amplitudes are substantially degraded relative to the "Truth" (Figs. S1-9) in 6 of the 9 models examined (MPI, GFDL-ESM2M and CESM1 are the exceptions.

This degradation in the regression amplitudes when the global-mean is included is nearly always associated with the presence of a forced component in the AMV Index timeseries (Fig. S17; MPI and GFDL-ESM2M are the two exceptions). The presence of a forced component is indicated

when the ensemble-mean (thick curves in Fig. S17) of the individual member AMV timeseries (thin curves in Fig. S17) differs significantly from zero at the 90% confidence level (i.e., when more than 10% of the members have non-zero values). For example, the AMV Index for MIROC6 contains a statistically significant sizeable forced component after about 2020 (panel f in Fig. S17). While the aim of subtracting G from NA was to remove any forced component from the AMV Index according to TS06, the procedure clearly falls short of its intended goal starting in the middle of the 21st century in the majority of model LEs we analyzed (Fig. S17).

To provide more quantitative information, we have calculated the proportion of internal-to-total variance in the individual AMV timeseries, and then averaged these proportions across all the members of a given model Large Ensemble. We did this calculation for both time periods (1950-2020 and 1950-2090) and have indicated the results as numerals in the upper right hand corner of each panel of Fig. S17. The proportion of internal-to-total variance in the individual AMV timeseries, on average, is notably close to unity (values < 1.4) during the period 1950-2090 in 6 of the 9 models, and also close to unity (values < 1.6) during 1950-2020 in 4 of the 9 models (Fig. S17). Thus, inferences about the proportion of internal variance in the observed AMV timeseries (also shown in Fig. S17) will depend on which model is used to estimate the forced contribution. For example, according to MPI, the observed record (during 1950-2020) would be interpreted as almost entirely unforced, while according to CanESM5, it would be interpreted as containing a sizeable forced component.

In summary, the results shown in Figs. S15-17 caution against implementing the TS06 method without first subtracting the global-mean from the gridded field before computing correlation or

86 regression maps with the AMV Index, especially when considering future time periods from model
87 projections. A second cautionary note is that the AMV Index itself as defined by TS06 (i.e., NA-
88 G SST) may contain a forced component, despite the intended goal of isolating the internal
89 component with this method.
90

2. References

Delworth, T. L., Cooke, W. F., Adcroft, A., Bushuk, M., Chen, J.-H., Dunne, K. A., et al. (2020). SPEAR: The next generation GFDL modeling system for seasonal to multidecadal prediction and projection. Journal of Advances in Modeling Earth Systems, 12, e2019MS001895. https://doi.org/10.1029/2019MS001895.

Deser, C., F. Lehner, K. B. Rodgers, T. Ault, T. L. Delworth, P. N. DiNezio, A. Fiore, C. Frankignoul, J. C. Fyfe, D. E. Horton, J. E. Kay, R. Knutti, N. S. Lovenduski, J. Marotzke, K. A. McKinnon, S. Minobe, J. Randerson, J. A. Screen, I. R. Simpson and M. Ting, 2020: Insights from earth system model initial-condition large ensembles and future prospects. *Nat. Clim. Change*, doi: 10.1038/s41558-020-0731-2.

Jeffrey, S. et al., 2013: Australia's CMIP5 submission using the CSIRO-Mk3. 6 model. *Aust. Meteorol. Ocean.* 63, 1–13.

Kay, J. E., C. Deser, A. Phillips, A. Mai, C. Hannay, G. Strand, J. Arblaster, S. Bates, G. Danabasoglu, J. Edwards, M. Holland, P. Kushner, J. -F. Lamarque, D. Lawrence, K. Lindsay, A. Middleton, E. Munoz, R. Neale, K. Oleson, L. Polvani, and M. Vertenstein, 2015: The Community Earth System Model (CESM) Large Ensemble Project: A community resource for studying climate change in the presence of internal climate variability. *Bull. Amer. Met. Soc.*, **96**, 1333–1349, doi: 10.1175/BAMS-D-13-00255.1.

Kirchmeier-Young, M. C., Zwiers, F. W. and Gillett, N. P. , 2017: Attribution of extreme events in Arctic Sea ice extent. *J. Climate* 30, 553–571.

Maher, N., Milinski, S., Suarez-Gutierrez, L., Botzet, M., Dobrynin, M., Kornblueh, L., et al. (2019). The Max Planck Institute Grand Ensemble: Enabling the exploration of climate system variability. *J. Adv. Mod. Earth Sys.*, 11, 2050– 2069. https://doi.org/10.1029/2019MS001639

Rodgers, K. B., Lin, J. & Frölicher, T. L. Emergence of multiple ocean ecosystem drivers in a large ensemble suite with an Earth system model. Biogeosciences 12, 3301–3320 (2015).

Rodgers, K. B., Lee, S.-S., Rosenbloom, N., Timmermann, A., Danabasoglu, G., Deser, C., Edwards, J., Kim, J.-E., Simpson, I., Stein, K., Stuecker, M. F., Yamaguchi, R., Bodai, T., Chung, E.-S., Huang, L., Kim, W., Lamarque, J.-F., Lombardozzi, D., Wieder, W. R., and Yeager, S. G., 2021: Ubiquity of human-induced changes in climate variability, *Earth Syst. Dynam,* https://doi.org/10.5194/esd-2021-50, 2021.

Sun, L., Alexander, M. and Deser, C. , 2018: Evolution of the global coupled climate response to Arctic sea ice loss during 1990–2090 and its contribution to climate change. *J. Climate* 31, 7823–7843.

Swart, N. C., Cole, J. N. S., Kharin, V. V., Lazare, M., Scinocca, J. F., Gillett, N. P., Anstey, J., Arora, V., Christian, J. R., Hanna, S., Jiao, Y., Lee, W. G., Majaess, F., Saenko, O. A., Seiler, C., Seinen, C., Shao, A., Sigmond, M., Solheim, L., von Salzen, K., Yang, D., and Winter, B.: The

Canadian Earth System Model version 5 (CanESM5.0.3), Geosci. Model Dev., 12, 4823–4873, https://doi.org/10.5194/gmd-12-4823-2019, 2019.

Tatebe, H., Ogura, T., Nitta, T., Komuro, Y., Ogochi, K., Takemura, T., Sudo, K., Sekiguchi, M., Abe, M., Saito, F., Chikira, M., Watanabe, S., Mori, M., Hirota, N., Kawatani, Y., Mochizuki, T., Yoshimura, K., Takata, K., O'Ishi, R., ... Kimoto, M. (2019). Description and basic evaluation of simulated mean state, internal variability, and climate sensitivity in MIROC6. *Geoscientific Model Development*, *12*(7), 2727-2765. https://doi.org/10.5194/gmd-12-2727-2019.

Trenberth, K. E., and Shea, D. J., 2006: Atlantic hurricanes and natural variability in 2005. *Geophy. Res. Lett.*, 33, L12704. https://doi.org/10.1029/2006GL026894.

3. Table

Table S1. Summary of the salient characteristics of the 9 model initial-condition Large Ensembles used in this study. "Macro" refers to different coupled initial states; "Micro" refers to different atmospheric initial states (see Deser et al., 2020).

Modeling Center	Model Version	Model Resolution (atm/ocn)	Years	Initialization Method	Number of Members	Forcing	Reference
CCCma	CanESM2	~2.8°x2.8°/ ~1.4°x0.9°	1950-2100	Macro and Micro	50	historical, rcp85	Kirchmeier-Young et al. (2017)
CSIRO	MK3.6	~1.9°x1.9°/ ~1.9°x1.0°	1850-2100	Macro	30	historical, rcp85	Jeffrey et al. (2013)
GFDL	ESM2M	~2.0°x2.5°/ ~1.0°x0.9°	1950-2100	Macro	30	historical, rcp85	Rodgers et al. (2015)
MPI	MPI-ESM-LR	~1.9°x1.9°/ nominal 1.5°	1850-2100	Macro	100	historical, rcp26, rcp45, rcp85	Maher et al. (2019)
NCAR	CESM1-CAM5	~1.3°x0.9°/ nominal 1.0°	1920-2100	Micro	40	historical, rcp85	Kay et al. (2015)
CCCma	CanESM5	~2.8°x2.8°/ ~1.4°x0.9°	1850-2100	Macro	50	historical, ssp5-8.5	Swart et al. (2019)
GFDL	SPEAR_MED	50km/ nominal 1°	1921-2100	Macro	30	historical, ssp5-8.5	Delworth et al. (2020)
MIROC	MIROC6	~1.4°x1.4°/ nominal 1°	1850-2014	Macro	50	historical, ssp5-8.5	Tatebe et al. (2019)
NCAR	CESM2	~1.3°x0.9°/ nominal 1.0°	1850-2100	Macro and Micro	100 (only members 51-90 used)	historical, ssp3-7.0	Rodgers et al. (2021)

4. Figures

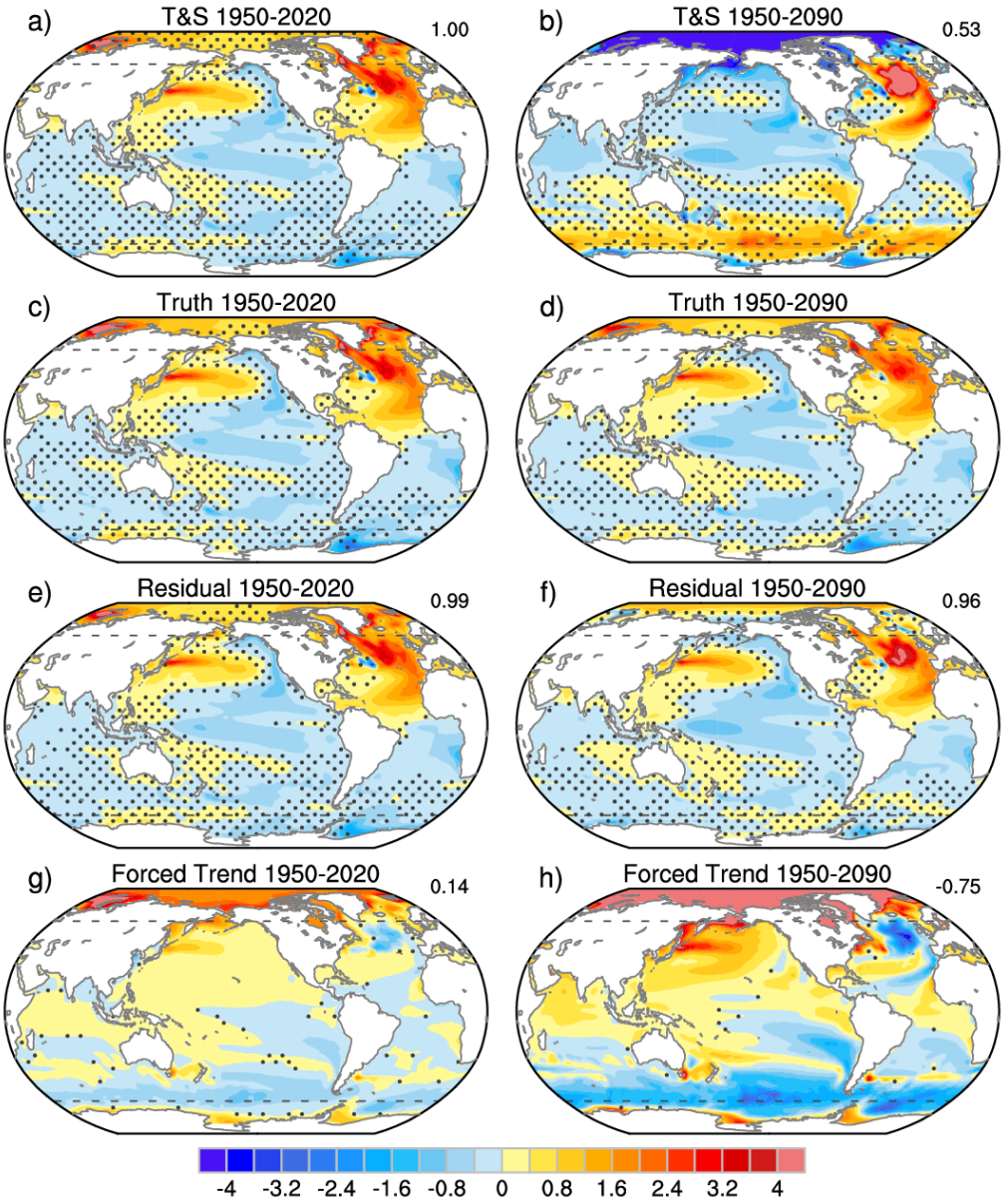

158

159 **Figure S1**. SST anomaly regression maps of internal Atlantic Multidecadal Variability (iAMV)
160 in the 100-member MPI Large Ensemble during (left) 1950-2020 and (right) 1950-2090. Panels
161 a,b (e,f) show estimates based on the T&S (Residual) method; panels c,d show the true patterns
162 ("Truth"). Stippled regions are not statistically significant at the 90% confidence level based on a
163 2-sided t-test. The number in the upper right of panels a,b and e,f denotes the pattern correlation
164 coefficient with the true iAMV for the corresponding time period based on the domain 60°S-60°N
165 (marked by dashed gray lines). Panels g and h show the forced (ensemble-mean) SSTA trends after
166 subtracting the global-mean (60°S-60°N) forced SSTA trends. The color bar is unitless for panels
167 a-f (°C per °C of the iAMV index) and in units of °C per 70 years for panel g and °C per 140 years
168 for panel h. The number in the upper right of panels g,h denotes the pattern correlation coefficient
169 with T&S for the corresponding time period. See main text for details.
170

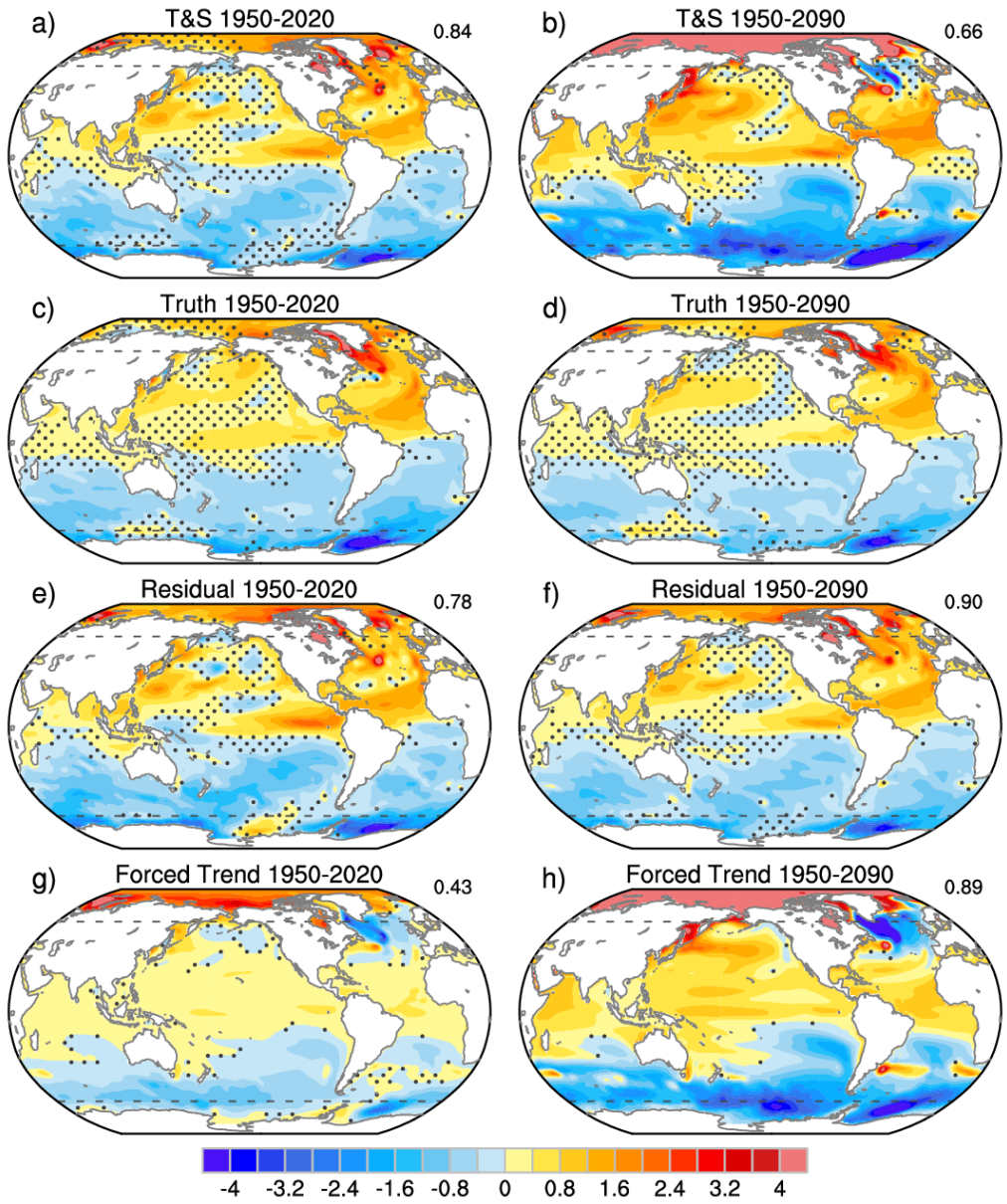

171
172
173 **Figure S2**. As in Fig. S1 but for the 30-member GFDL-ESM2M Large Ensemble.

174

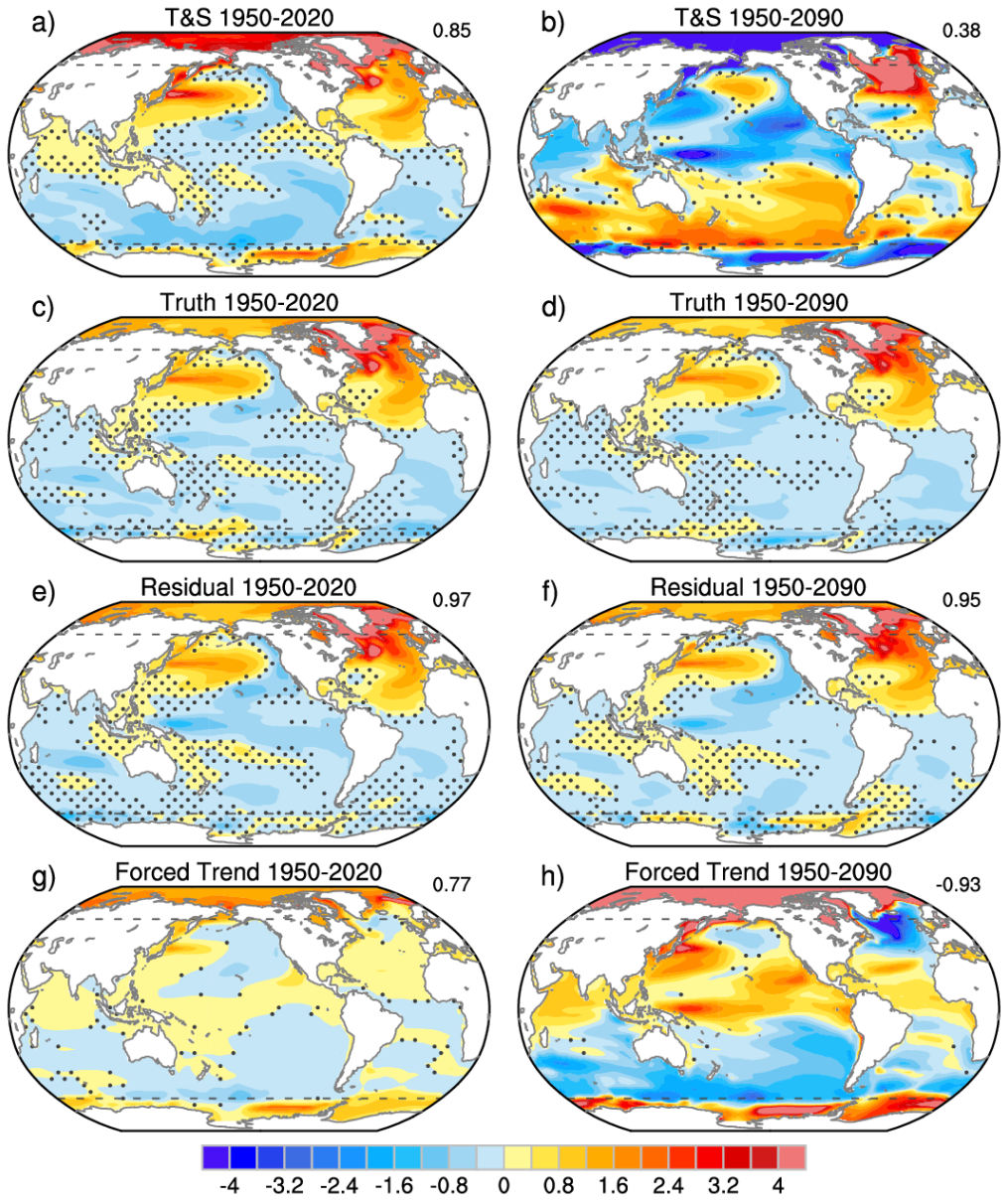

175
176

177 **Figure S3**. As in Fig. S1 but for the 30-member CSIRO Large Ensemble.

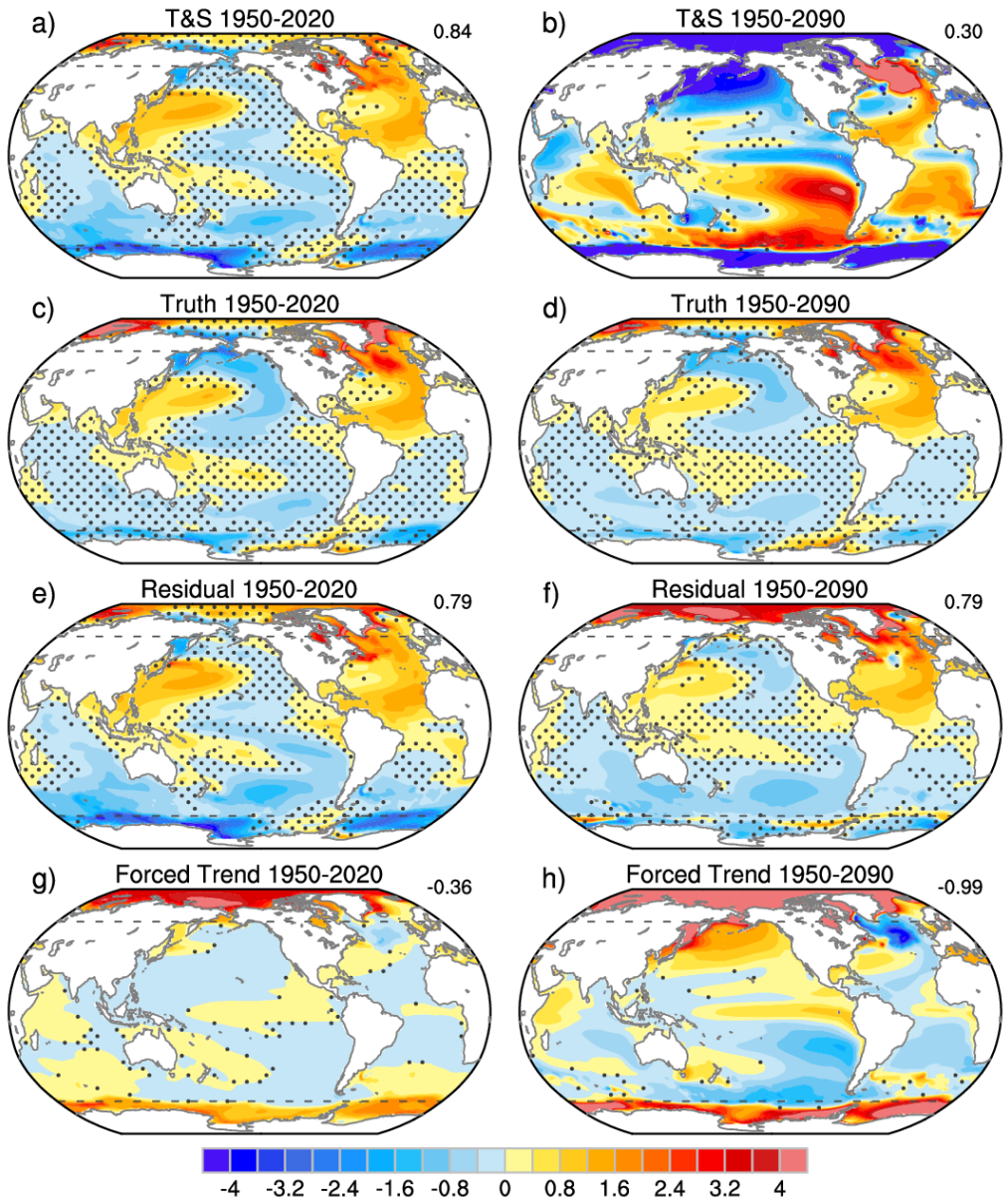

178
179

180 **Figure S4**. As in Fig. S1 but for the 40-member CESM1 Large Ensemble.

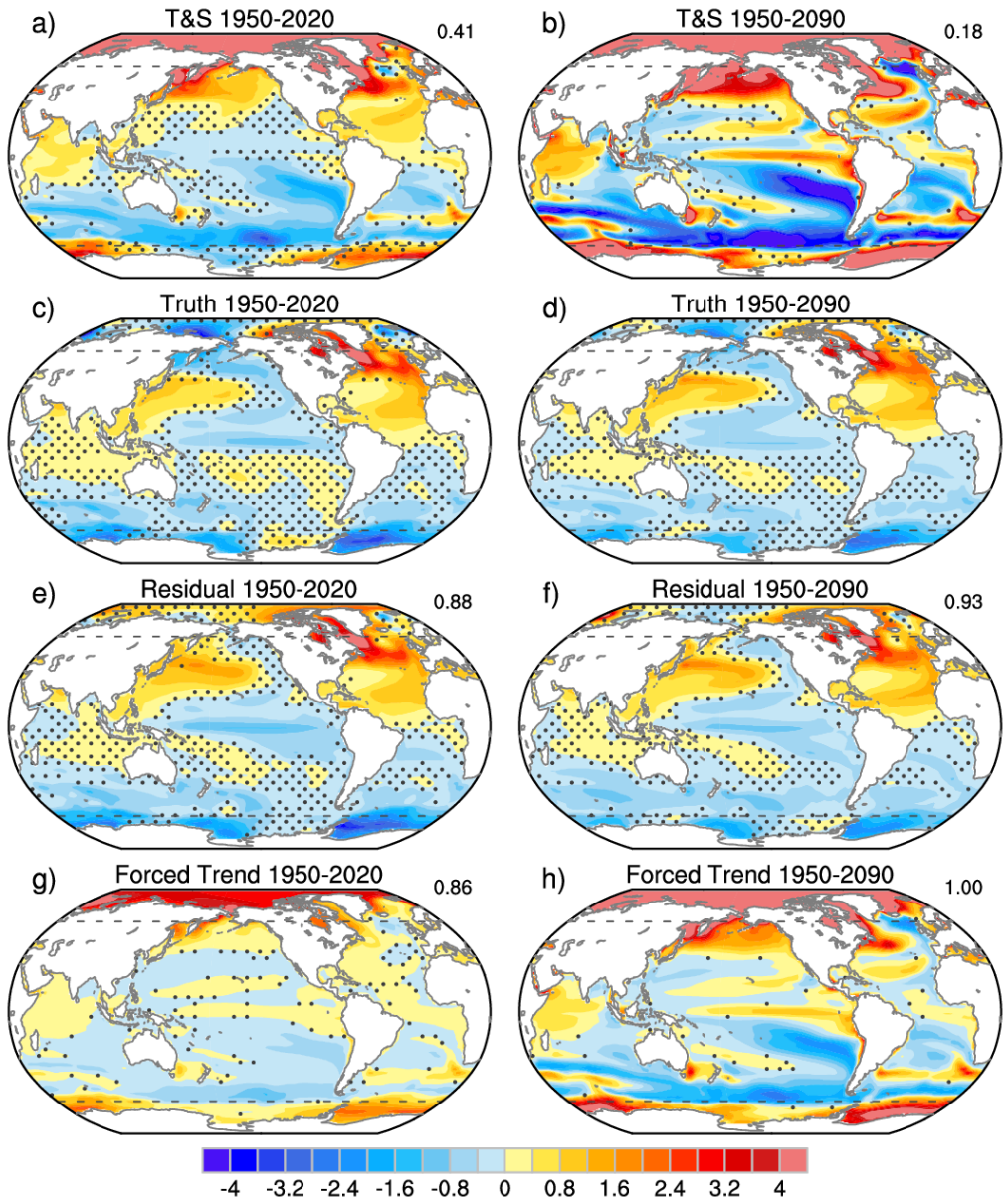

181
182

183 **Figure S5**. As in Fig. S1 but for the 50-member CanESM2 Large Ensemble.

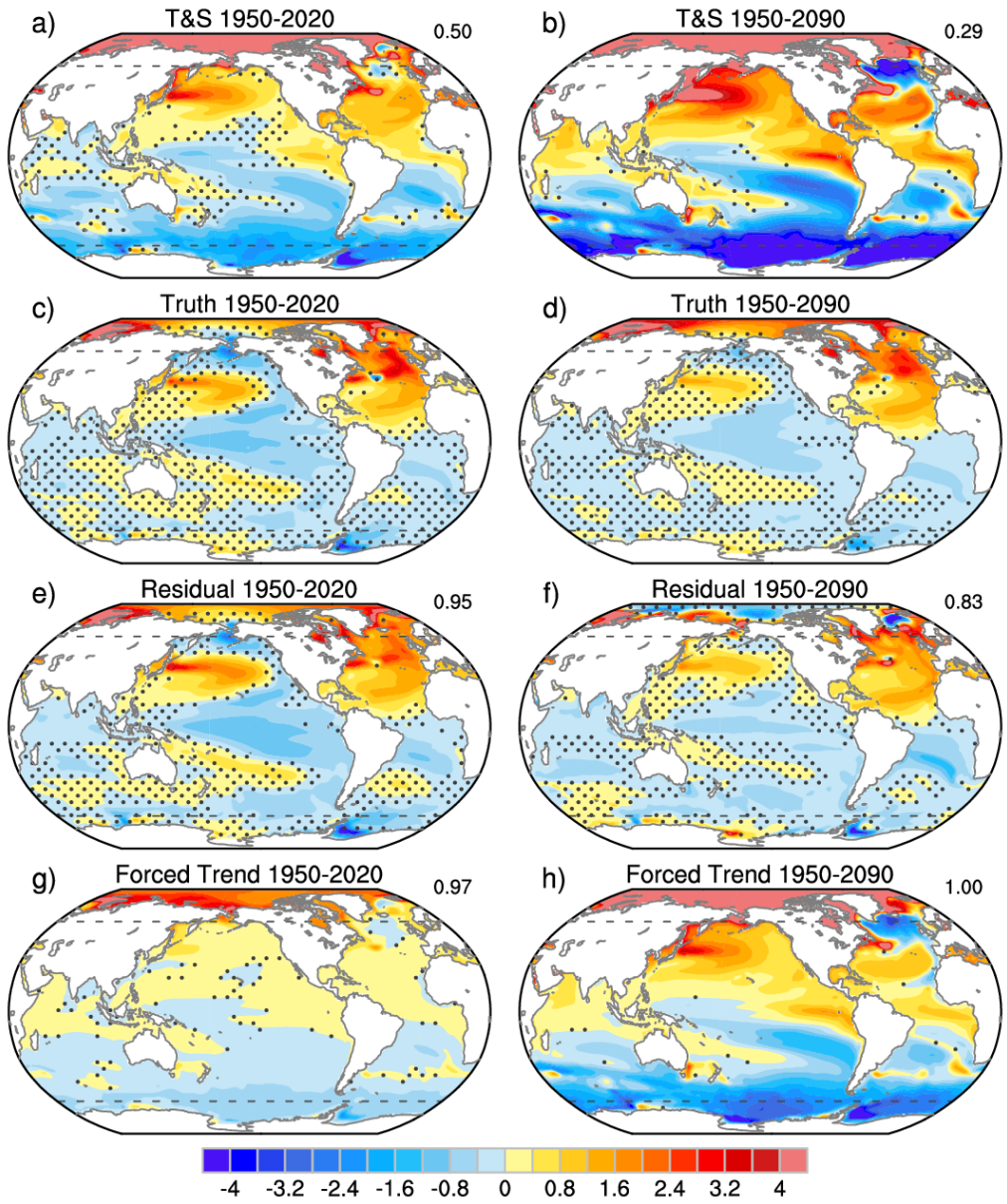

184
185

186 **Figure S6**. As in Fig. S1 but for the 50-member MIROC6 CMIP6 Large Ensemble.

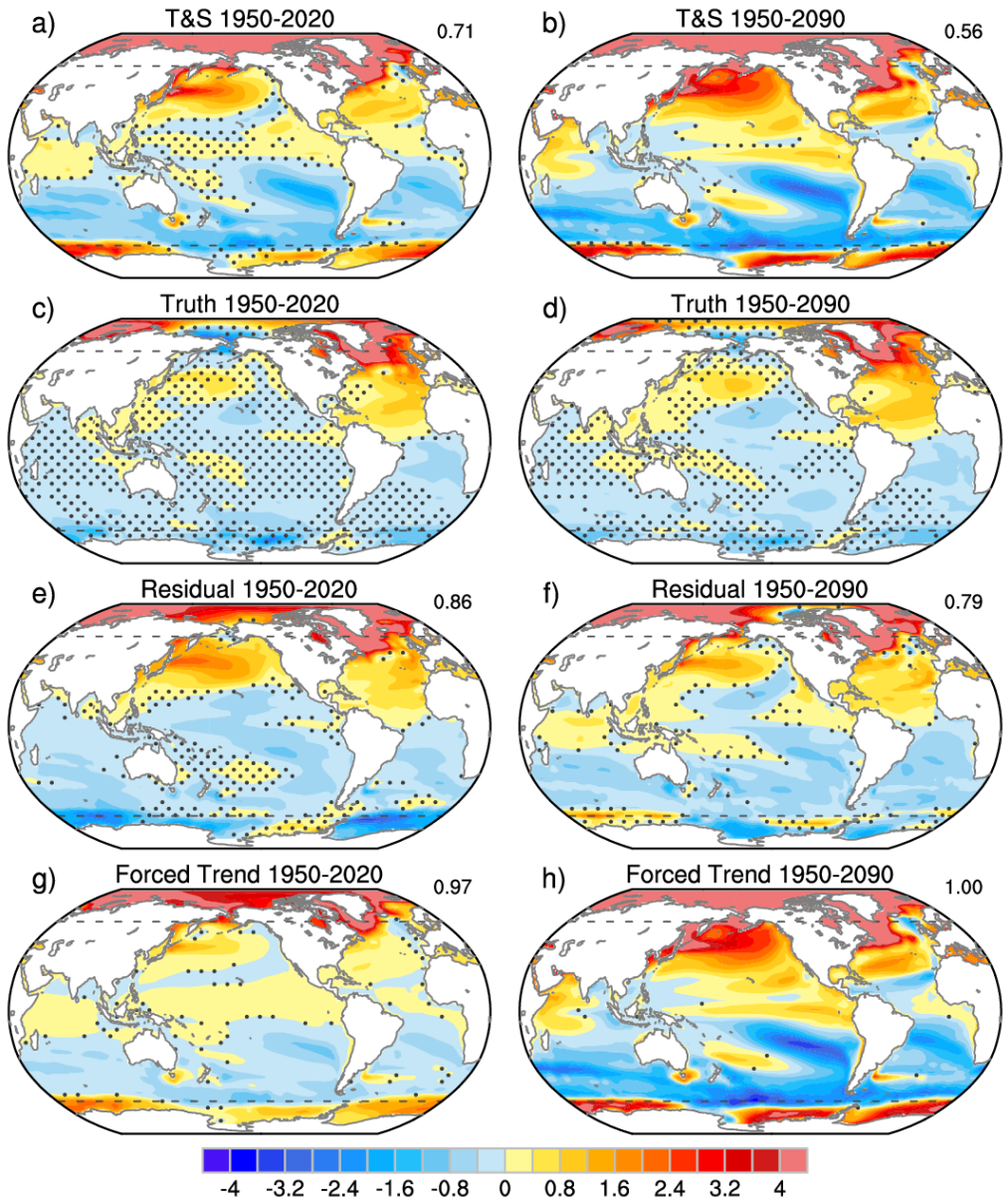

187
188

189 **Figure S7**. As in Fig. S1 but for the 50-member CanESM5 Large Ensemble.

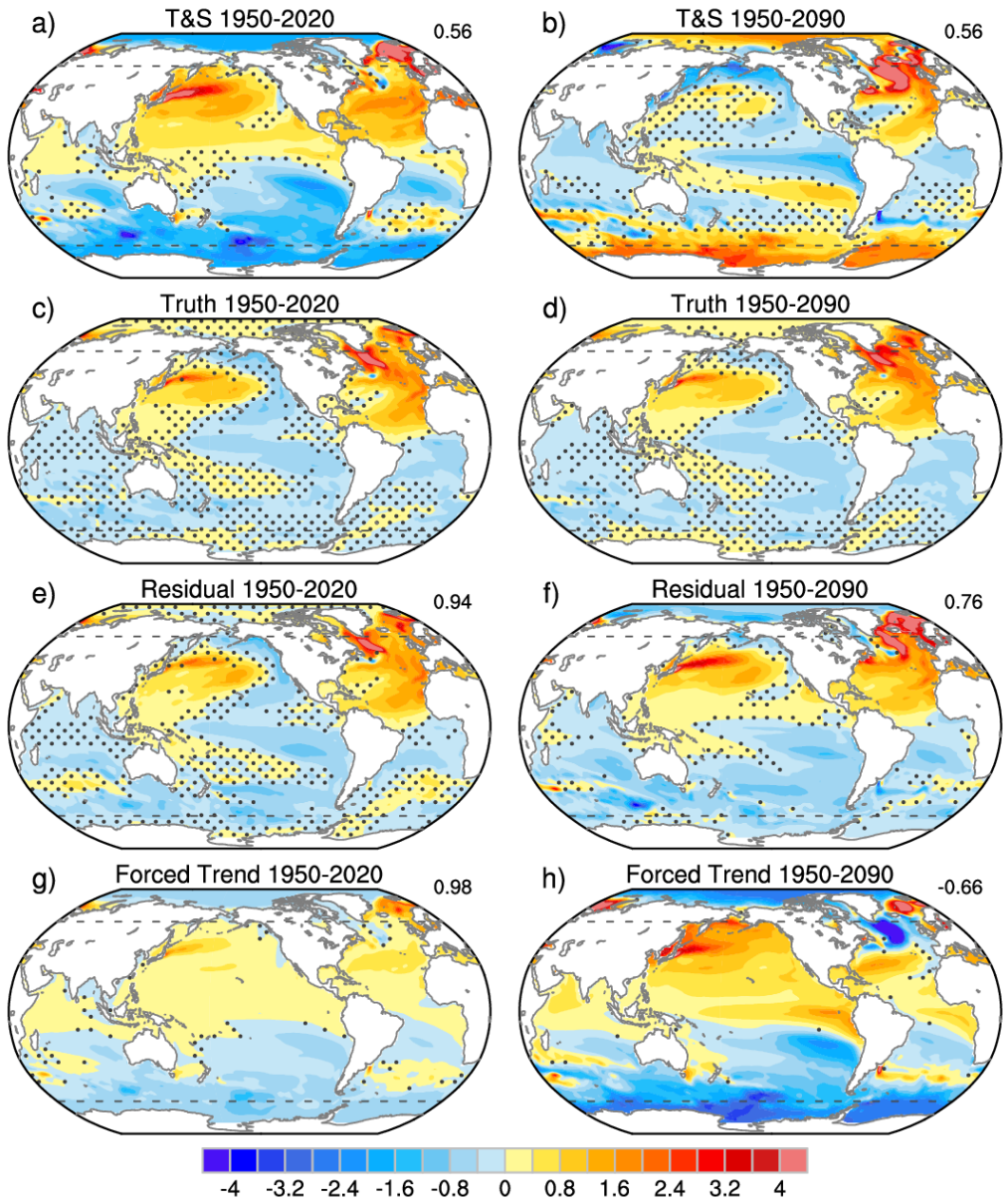

Figure S8. As in Fig. S1 but for the 30-member GFDL SPEAR_MED Large Ensemble.

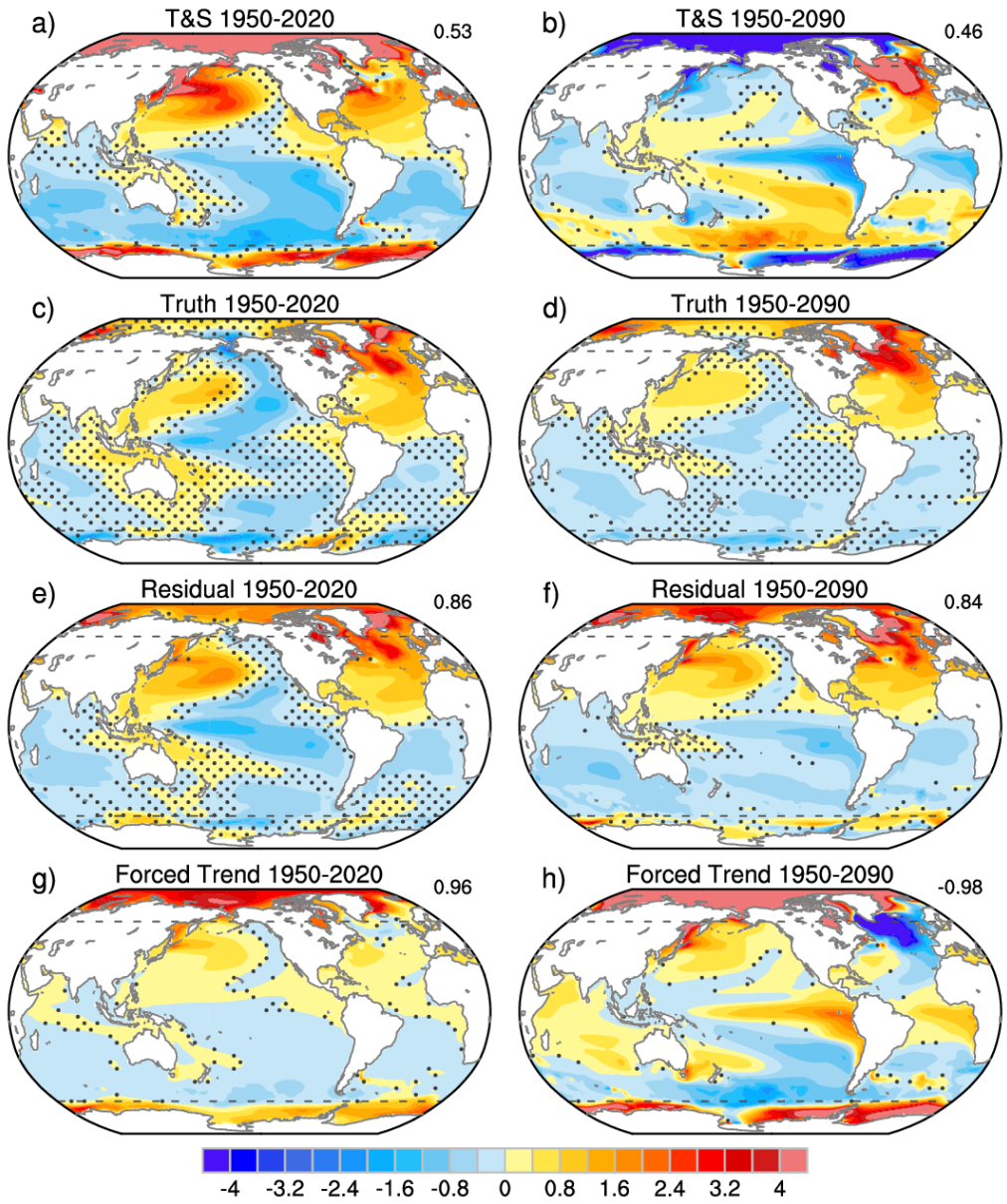

Figure S9. As in Fig. S1 but for the 40-member CESM2 Large Ensemble.

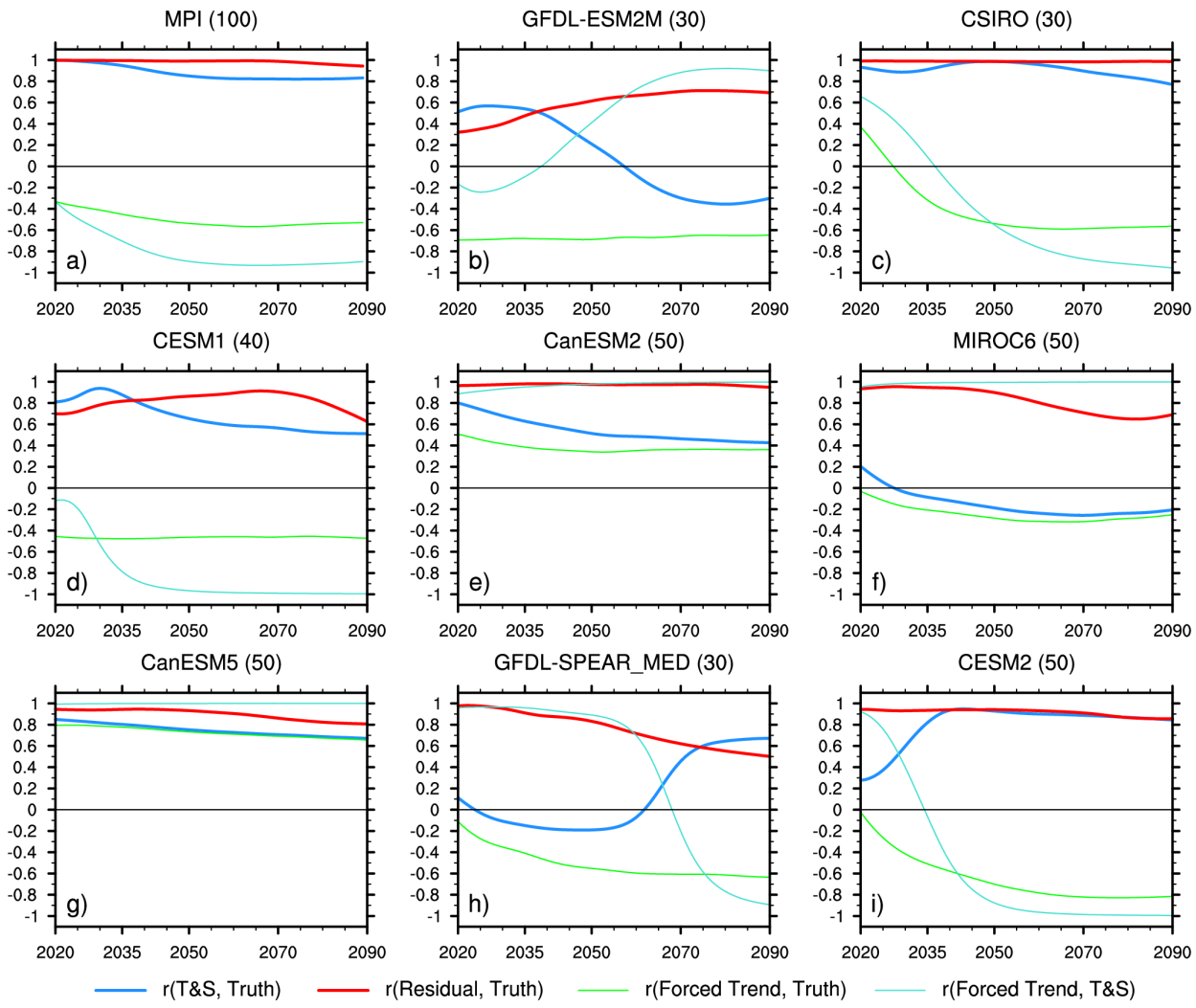

Figure S10. Cumulative pattern correlation coefficients between iAMV SST anomaly regression maps computed over the North Atlantic domain (0°-60°N, 80°W-0°E) based on: T&S method *vs*. Truth (blue curves); Residual method *vs*. Truth (red curves); Forced trend *vs*. T&S method (cyan curves); Forced trend *vs*. Truth (green curves). Each analysis period begins in 1950 and ends in the year labeled along the x-axis (i.e., 2020 denotes the period 1950-2020, 2021 the period 1950-2021, etc.). Each panel shows a different model Large Ensemble, with the number of ensemble members indicated in parentheses (see Table S1).

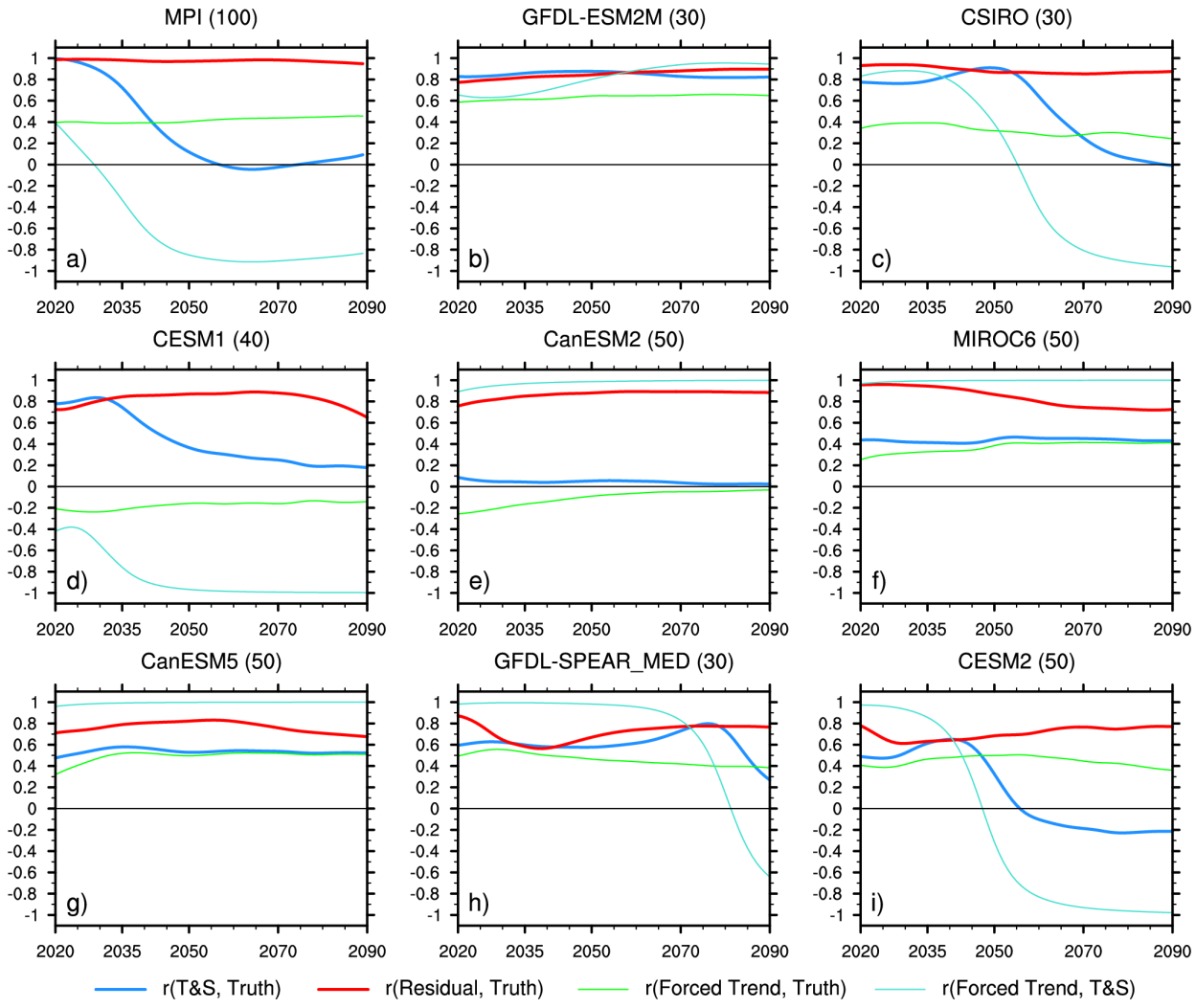

Figure S11. As in Fig. S10 but based on the global domain (60°S-60°N) exclusive of the North Atlantic (0°-60°N, 80°W-0°E).

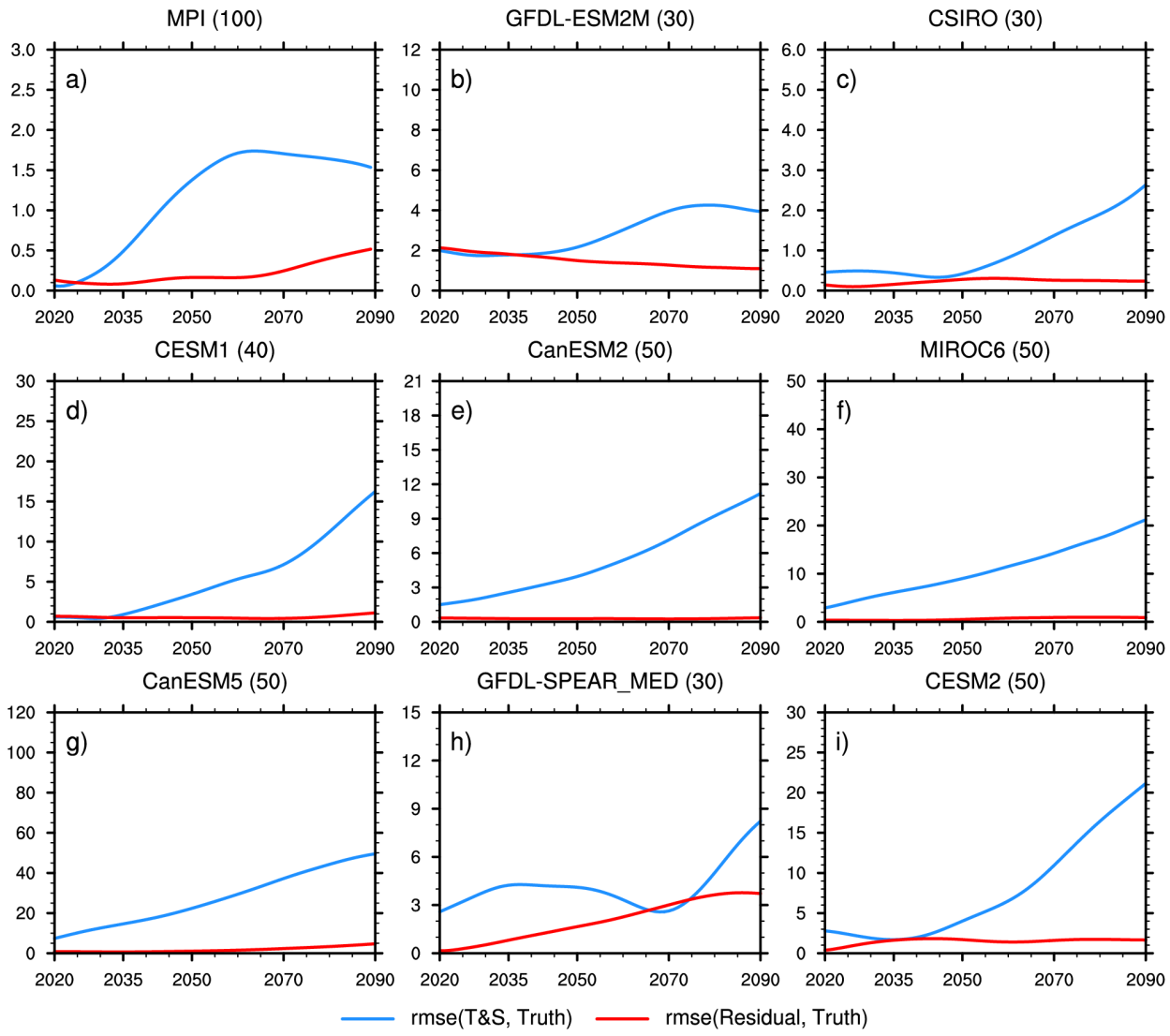

Figure S12 As in Fig. S10 but for cumulative spatial rms differences relative to the spatial rms of the true *iAMV* regression map ("rmse") for each model Large Ensemble. Blue curves: T&S method *vs.* Truth; red curves: Residual method *vs.* Truth.

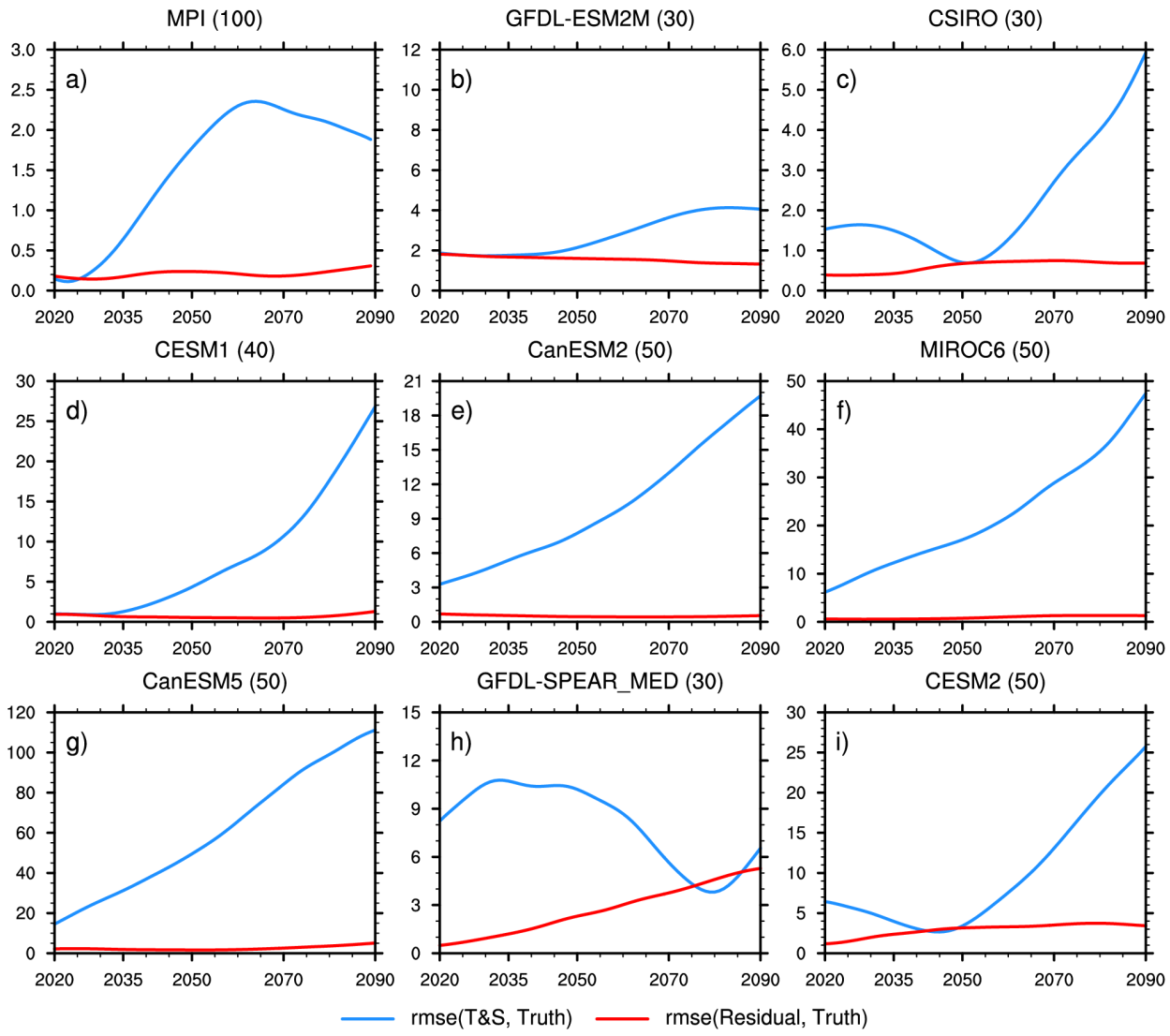

Figure S13. As in Fig. S11 but for cumulative spatial rms differences relative to the spatial rms of the true *iAMV* regression map ("rmse") for each model Large Ensemble. Blue curves: T&S method *vs.* Truth; red curves: Residual method *vs.* Truth.

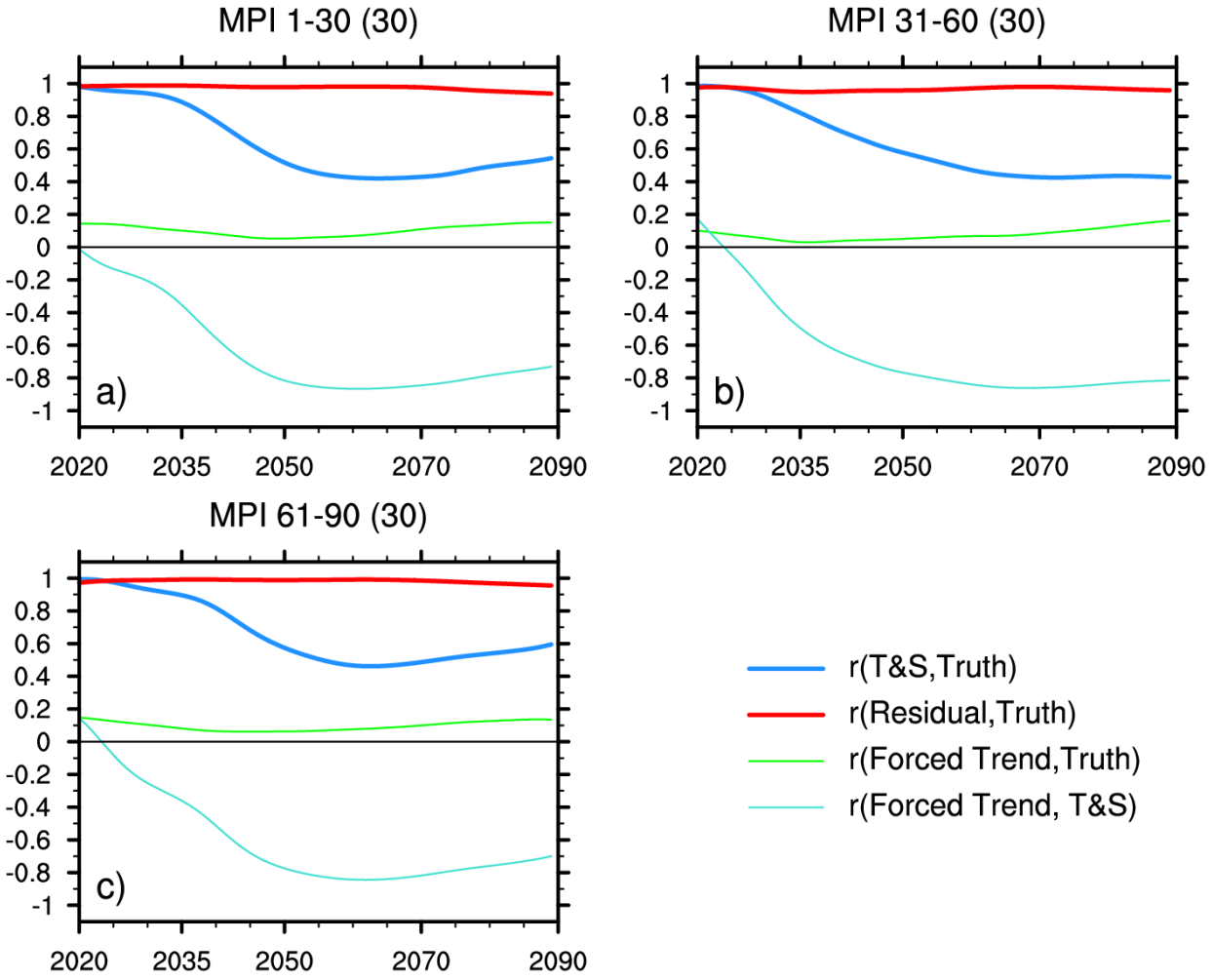

Figure S14. Cumulative pattern correlation coefficients between iAMV SST anomaly regression maps over the domain 60°S-60°N for 30-member subsets of the 100-member MPI Large Ensemble based on: T&S method *vs*. Truth (blue curves); Residual method *vs*. Truth (red curves); Forced trend *vs*. T&S method (cyan curves); Forced trend *vs*. Truth (green curves). The cumulative analysis periods begin in 1950 and end in the year labeled along the x-axis (i.e., 2020 denotes the period 1950-2020, 2021 the period 1950-2021, etc.). Members (a) 1-30; (b) 31-60; and (c) 61-90.

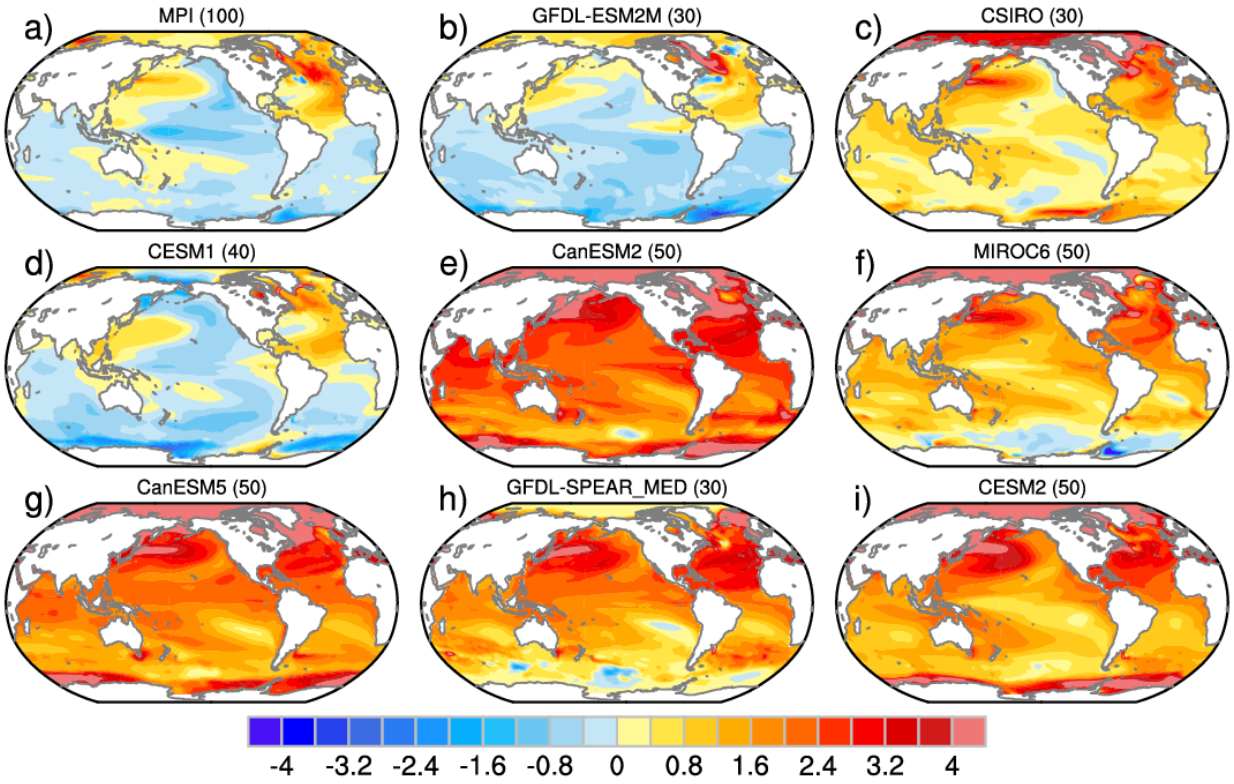

Figure S15. SST anomaly regression maps of internal Atlantic Multidecadal Variability based on the Trenberth and Shea (2006) method for each model Large Ensemble based on the period 1950-2020; note that global-mean SST has not been subtracted before computing the regression coefficients onto the NA-G SST Index (see text for details). All data are annual means and have been low-pass filtered with a 20-year Butterworth Filter. The color bar is unitless (°C per °C of the NA-G index).

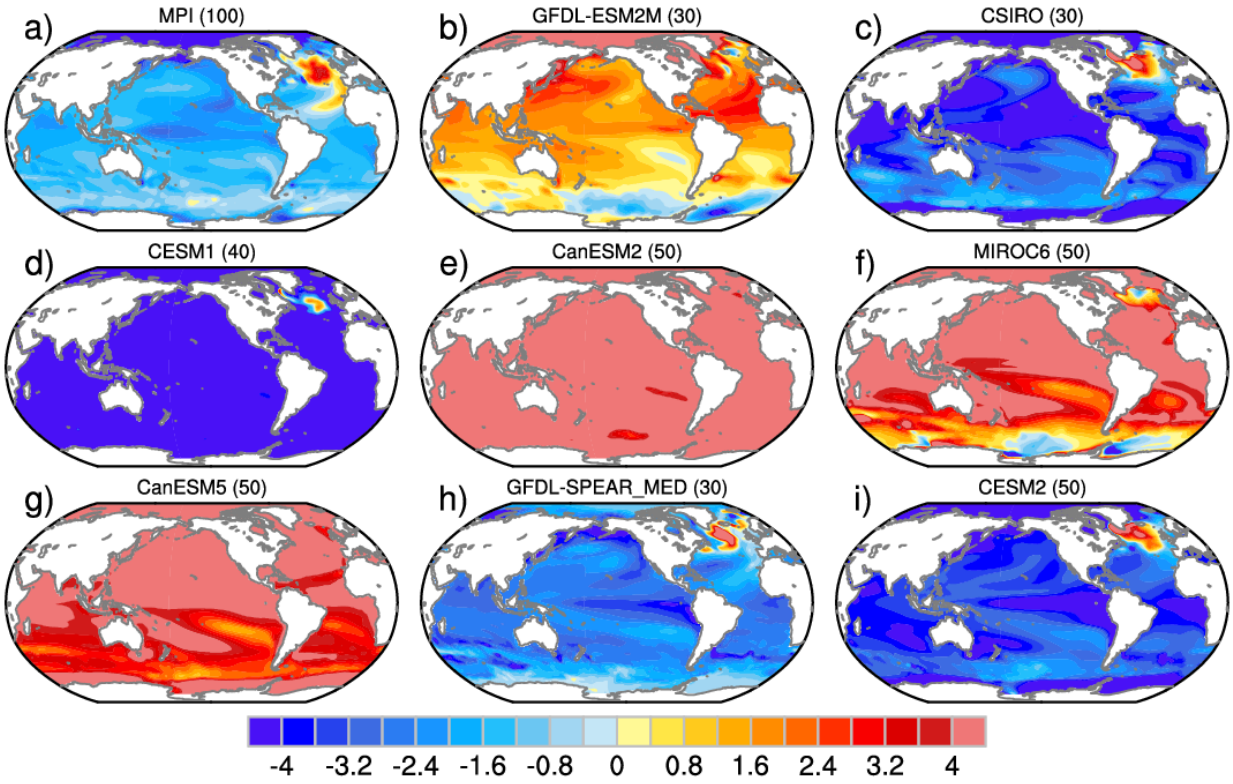

Figure S16. As in Fig. S15 but for the period 1950-2090.

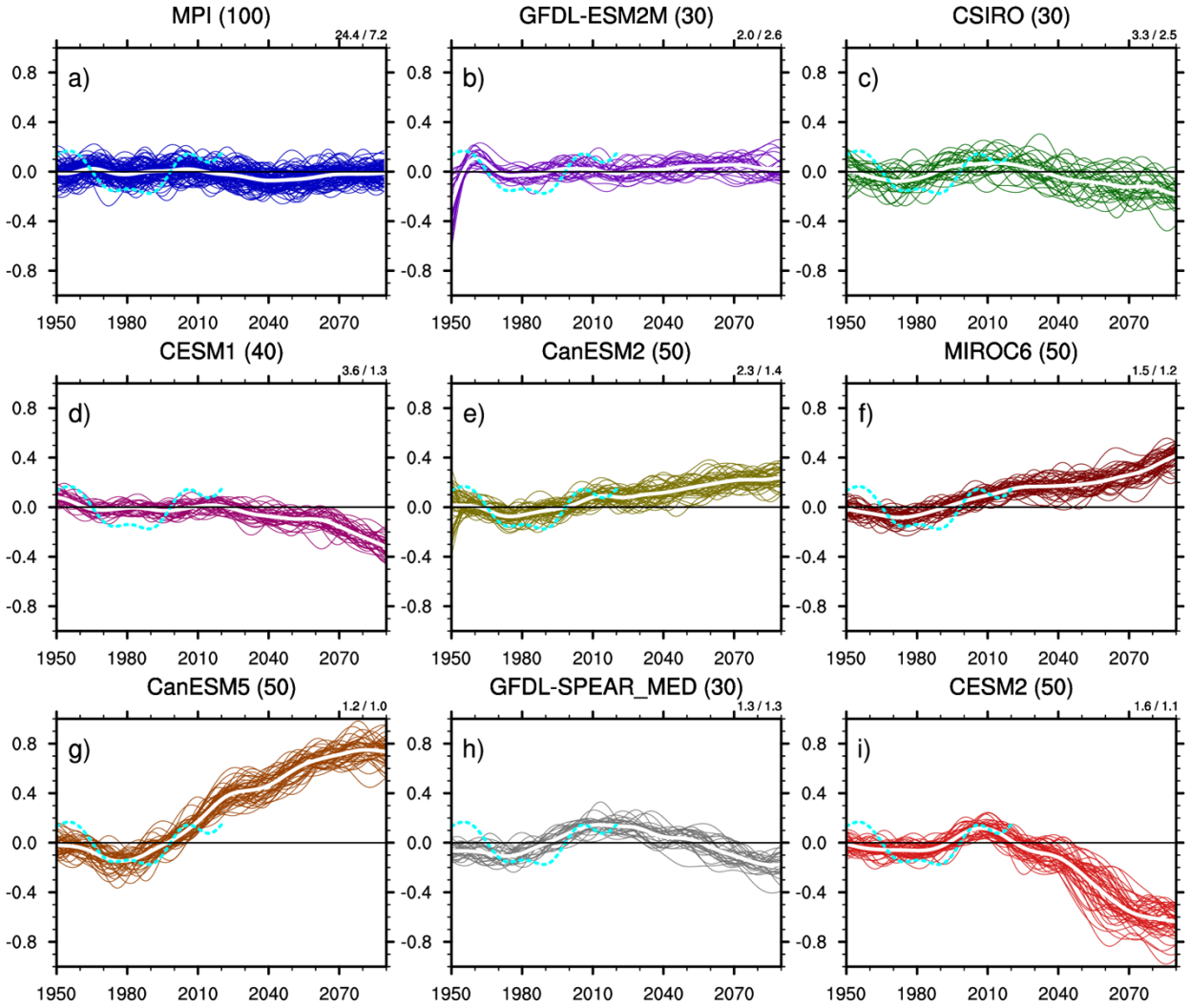

Figure S17. Timeseries (°C) of NA-G SST in each model Large Ensemble for the period 1950-2090. Thin curves show the individual ensemble members; thick white curves show the average of the thin curves. The thick dashed cyan curve shows the observed NA-G SST timeseries based on ERSSTv5. All data are annual means and have been low-pass filtered with a 20-year Butterworth Filter. Numbers in the upper right of each panel denote the proportion of internal-to-total variance, on average across the individual members. The first number is based on the period 1950-2020 and the second number (after the forward slash) is based on 1950-2090.